

Surfactant Micelle-Driven High-Efficiency and High-Resolution Length Separation of Carbon Nanotubes for Electronic Applications

Shuang Ling, Xiaojun Wei,* Xin Luo, Xiao Li, Shilong Li, Feibing Xiong,* Weiya Zhou, Sishen Xie, and Huaping Liu*

High-efficiency extraction of long single-wall carbon nanotubes (SWCNTs) with excellent optoelectronic properties from SWCNT solution is critical for enabling their application in high-performance optoelectronic devices. Here, a straightforward and high-efficiency method is reported for length separation of SWCNTs by modulating the concentrations of binary surfactants. The results demonstrate that long SWCNTs can spontaneously precipitate for binary-surfactant but not for single-surfactant systems. This effect is attributed to the formation of compound micelles by binary surfactants that squeeze the free space of long SWCNTs due to their large excluded volumes. With this technique, it can readily separate near-pure long (≥ 500 nm in length, 99% in content) and short (≤ 500 nm in length, 98% in content) SWCNTs with separation efficiencies of 26% and 64%, respectively, exhibiting markedly greater length resolution and separation efficiency than those of previously reported methods. Thin-film transistors fabricated from extracted semiconducting SWCNTs with lengths > 500 nm exhibit significantly improved electrical properties, including a 10.5-fold on-state current and 14.7-fold mobility, compared with those with lengths < 500 nm. The present length separation technique is perfectly compatible with various surfactant-based methods for structure separations of SWCNTs and is significant for fabrication of high-performance electronic and optoelectronic devices.

biomedicine.^[1–3] For example, SWCNTs with nanoscale diameters are considered one of the most ideal materials for fabricating high-speed, power-efficient, and high-performance thin-film transistors (TFTs) because of their extremely high carrier mobility, tunable direct bandgaps, and solution processability.^[4–7] The performance of semiconducting SWCNT-based TFTs has been proven to exceed that of silicon-based devices of the same size,^[8] which provides a promising path toward beyond-silicon electronic systems. To produce semiconducting SWCNTs from as-grown products that generally contain semiconducting and metallic SWCNTs, various liquid separation methods, including polymer wrapping,^[9,10] density gradient ultracentrifugation (DGU),^[11,12] gel chromatography,^[13–15] and aqueous two-phase extraction (ATP),^[16,17] have been developed over the past two decades. Through continuous development and improvement, these methods have achieved the separation of high-purity single-chirality SWCNTs,^[18–24] and even specific SWCNT enantiomers.^[25–31]

Before structural separation by a liquid method, it is necessary to prepare SWCNTs by mono-dispersion in aqueous or organic solution.^[32] To achieve high-efficiency dispersion, an additional sonication treatment is widely used because as-grown SWCNTs

1. Introduction

Due to their excellent electrical, optical, and mechanical properties, single-wall carbon nanotubes (SWCNTs) have broad application prospects in the fields of information, energy, and

S. Ling, X. Wei, X. Luo, X. Li, S. Li, W. Zhou, S. Xie, H. Liu
Beijing National Laboratory for Condensed Matter Physics
Institute of Physics
Chinese Academy of Sciences
Beijing 100190, China
E-mail: weixiaojun@iphy.ac.cn; liuhuaping@iphy.ac.cn

S. Ling, F. Xiong
Department of Optoelectronic
Xiamen University of Technology
Xiamen, Fujian 361024, China
E-mail: fbxiong@xmut.edu.cn

X. Wei, X. Li, W. Zhou, S. Xie, H. Liu
Department of Physics and Center of Materials Science and
Optoelectronics Engineering
University of Chinese Academy of Sciences
Beijing 100049, China

X. Wei, X. Li, S. Li, W. Zhou, S. Xie, H. Liu
Beijing Key Laboratory for Advanced Functional Materials and Structure
Research
Beijing 100190, China

X. Wei, W. Zhou, S. Xie, H. Liu
Songshan Lake Materials Laboratory
Dongguan, Guangdong 523808, China

 The ORCID identification number(s) for the author(s) of this article can be found under <https://doi.org/10.1002/sml.202400303>

DOI: 10.1002/sml.202400303

usually exist in the form of bundles due to strong van der Waals interactions. Unfortunately, the vigorous external force generated by sonication inevitably introduces defects on the surface of SWCNTs, degrading their inherent properties.^[33] Moreover, the length of isolated SWCNTs decreases, and the length typically ranges from hundreds of nanometers to a few micrometers. The presence of a large number of short nanotubes in SWCNT films negatively affects the performance of the corresponding electronic and optoelectronic devices due to the formation of many tube/tube junctions.^[34] Therefore, how to efficiently extract long SWCNTs with low defects from the monodispersed SWCNT solutions is a key for fabricating high-performance electronic and optoelectronic devices.

To achieve this goal, several methods, including size exclusion chromatography (SEC),^[29,35–39] DGU,^[40,41] field-flow fractionation,^[42] molecular crowding,^[43,44] have been developed for the length separation of SWCNTs. Although these methods can achieve length separation of SWCNTs, their length resolution capabilities remain insufficient. The long-SWCNT samples obtained by these methods usually contain many short SWCNTs (e.g., <500 nm in length), which can be confirmed by the presented length distribution for separated SWCNTs. In addition to the length resolution, the separation efficiency, which can be defined as the ratio of the amount of obtained long (or short) SWCNTs to that of the initial SWCNTs before separation, is another important factor for evaluating the effectiveness of length separation. Many groups, including ours, have employed SEC for the length separation of SWCNTs because SEC is a mature method that has been widely used for the extraction of various biomedical molecules. Based on our experience, the separation efficiency of SEC is generally very limited (typically $\approx 5\%$), and this efficiency is difficult to improve because the target SWCNTs must be fractionated into multiple species based on the length-dependent retention time in the stationary phase to obtain a relatively good fractionation effect.^[29] For other methods, the separation efficiencies are generally also very limited, so the detailed separation efficiency has rarely been demonstrated in previous reports. In addition, the requirement of expensive equipment (such as liquid chromatography or ultracentrifugation) may limit the practicality of several methods. Despite these challenges, a high-efficiency and high-resolution method for length separation of SWCNTs is highly desired to achieve their high-performance optoelectronic applications.

In this work, we report a straightforward method for the selective extraction of long SWCNTs without equipment requirements based on binary-surfactant systems. By modulating the concentration of binary surfactants (such as sodium dodecyl sulfate (SDS) and sodium cholate (SC), which are widely used for the dispersion and separation of SWCNTs), relatively long SWCNTs could spontaneously precipitate. Interestingly, after removing the relatively short SWCNTs in the supernatant, the precipitated long SWCNTs are dispersible only by handshaking, demonstrating that the process is reversible. Furthermore, this spontaneous precipitation of long SWCNTs does not occur in the single-surfactant SDS or SC system, and the proportion of precipitated SWCNTs increases with increasing surfactant and SWCNT concentration. These results revealed that the selective precipitation of long SWCNTs is induced by the surfactant micelles formed by SDS and SC, which significantly reduced the free space available

to the long SWCNTs due to their larger excluded volumes than short SWCNTs. Compared with all the previous methods, the present method exhibited a much greater length resolution and separation efficiency and achieved the separation of near-pure long (≥ 500 nm in length, 99% in content) and short (≤ 500 nm in length, 98% in content) SWCNTs with separation efficiencies of 26% and 64%, respectively. The average length of the obtained long SWCNTs reached ≈ 1 μm , which was significantly greater than previous results. The electrical measurements further demonstrated that the on-state current and mobility of TFTs fabricated from long semiconducting SWCNTs were 10.5 and 14.7 times greater than those of TFTs fabricated from short semiconducting SWCNTs. Our present technique for high-efficiency and high-resolution length separation lays a foundation for realizing high-performance electronic and optoelectronic applications of SWCNTs.

2. Results and Discussion

2.1. Selective Precipitation of Long SWCNTs Based on Binary-Surfactant Systems

In our previous experiments on the structure separation of SWCNTs via gel chromatography, we noticed that the separation results were strongly dependent on the freshness of the SWCNT dispersion.^[45] If the time interval between dispersion and separation is too long (such as several days), the adsorbabilities of SWCNTs on gels become very weak and uncontrollable. This unexpected phenomenon is especially pronounced for SWCNTs dispersed in binary-surfactant systems. Because the gel medium used is usually fresh, the most likely explanation is the change in the dispersion state of SWCNTs. In addition, if the surfactant concentration is too high (e.g., 5%), the dispersibility of SWCNTs will also deteriorate, resulting in the formation of nanotube bundles and reducing the shelf life of SWCNT dispersions. Therefore, we propose that the instability of the SWCNT dispersion may be caused by the surfactants. It is well known that binary surfactant molecules can easily form compound micelles when the concentrations exceed their critical micelle concentrations.^[46] The formed compound micelle with a much larger volume than a single surfactant molecule may decrease the free volume available for individual SWCNTs, and thus affect the dispersion state of SWCNTs. To clarify these doubts, we purposefully investigated the dispersion state of SWCNTs in binary surfactants, SDS and SC, which are widely used for the dispersion and separation of SWCNTs.

First, we prepared an arc-discharge SWCNT dispersion in a 1% SC solution by using traditional ultrasonication and ultracentrifugation methods (the details are described in the Experimental Section). After that, another surfactant, SDS, was added to the prepared SWCNT dispersion to create a binary-surfactant system in which the concentrations of SDS and SC were 2% and 0.2%, respectively, as typical conditions. As we predicted, the dispersion state of the SWCNTs clearly changed within 48 h. **Figure 1a** shows photographs of SWCNT dispersions after standing for various durations (0–48 h). It is clear that a large number of flocculent SWCNTs appear after 8 h compared with the pristine homogeneous dispersion and then gradually precipitate to the bottom of the container. After 20 h of standing, no additional

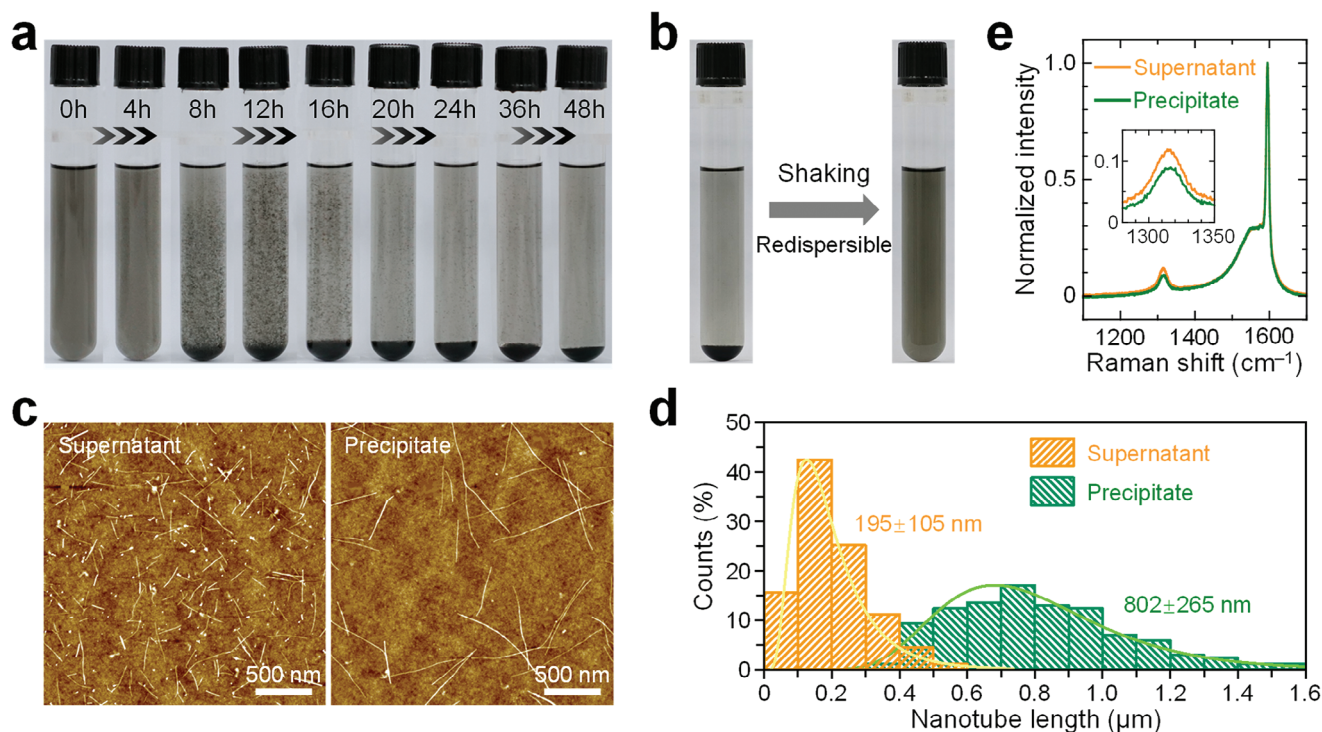


Figure 1. a) Photographs of SWCNT dispersions in a binary-surfactant system of 2% SDS + 0.2% SC after standing for various durations (0–48 h). b) Photographs of SWCNT dispersion (after standing for 48 h) before and after redispersion by handshaking. c,d) Typical AFM images c) and corresponding length distributions d) for SWCNTs contained in the supernatant and precipitate. e) Raman spectra of SWCNTs contained in the supernatant and precipitate at an excitation wavelength of 633 nm, in which each spectrum was normalized by the maximum intensity of the G^+ band. Inset: enlarged spectra of the D mode region.

flocculent SWCNTs formed, and most of the flocculent SWCNTs precipitated, indicating an approximately stable state. If we adopt a low-speed centrifugation treatment, the formation and precipitation of flocculent SWCNTs can be accelerated (Figure S1, Supporting Information), but these SWCNTs unexpectedly precipitate to the sidewall of the container due to the use of a fixed-angle rotor in the centrifugation process. In contrast to the well-known precipitation of SWCNTs induced by methanol or ethanol addition for divesting dispersant molecules coated onto the nanotube surfaces,^[47] the present precipitation is spontaneous in a binary-surfactant environment without any additive. Furthermore, the precipitated SWCNTs are redispersible upon shaking vessels by hand, as shown in Figure 1b, demonstrating a reversible process that is very important for subsequent purification and application. After removing the supernatant by pipette, the precipitated SWCNTs were redispersed into a fresh surfactant solution for subsequent morphological and spectral characterization. Figure 1c shows typical atomic force microscopy (AFM) images of the supernatant and precipitate. The data clearly show that the lengths of the SWCNTs in the precipitate are much longer than those in the supernatant. Additional AFM images of the SWCNTs contained in the supernatant, precipitate, and pristine dispersion before precipitation are shown in Figure S2 (Supporting Information). After systematically determining the length distribution of these SWCNTs, the average length was estimated to be 195 ± 105 nm for the supernatant, 802 ± 265 nm for the precipitate, and 391 ± 235 nm for the pristine SWCNTs (Figure 1d; Figure

S3, Supporting Information). The Raman spectral data further demonstrated the difference in the intensity ratio of G^+ to the defect band (Figure 1e; Figure S4, Supporting Information), indicating that the defect content of SWCNTs in the precipitates is lower than that in the supernatant. This result is consistent with the AFM observation because the defect content of SWCNTs is directly related to their length.

2.2. Effect of Binary Surfactants on Length-Selective Precipitation and Mechanism of Compound Micelles

Previous studies have demonstrated that the surfactant concentration strongly affects the structural selectivity of various liquid-phase separation methods.^[2] In the present binary-surfactant system, the surfactant concentration is further found to affect the precipitation amount and length of the precipitated SWCNTs. When the SC concentration in the SDS + SC system was fixed at 0.2%, the precipitation of SWCNTs did not occur at low SDS concentrations (0.2–1.0%) but occurred at high SDS concentrations (1.5–3.0%), as shown in Figure 2a. To estimate the proportion of precipitated SWCNTs and evaluate the separation efficiency, we redispersed the precipitated SWCNTs into a fresh surfactant solution after removing the supernatant by pipette. Considering the optical absorbance at 280 nm of the supernatant and precipitate (A_{280}^S and A_{280}^P , as SWCNT concentration) and their volumes (V^S and V^P), the proportions of the supernatant and precipitate

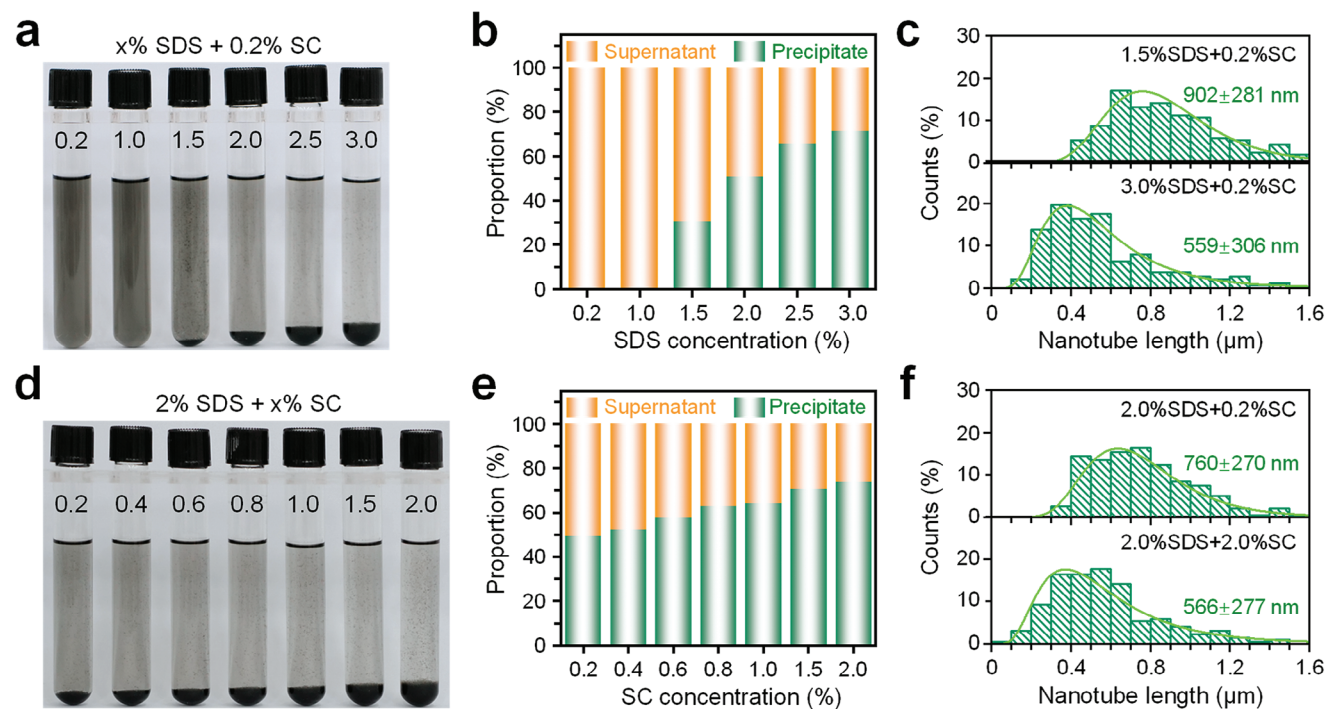


Figure 2. a,d) Photographs of SWCNT dispersions after 48 h of standing for binary-surfactant systems of x% SDS + 0.2% SC a) and 2% SDS + x% SC d). b,e) Proportions of the supernatant and precipitate at different SDS b) and SC e) concentrations. c,f) Length distributions of SWCNTs precipitated at 1.5% SDS + 0.2% SC and 3.0% SDS + 0.2% SC c), and at 2.0% SDS + 0.2% SC and 2.0% SDS + 2.0% SC d).

to the total SWCNTs at each surfactant concentration were calculated ($\frac{A_{280}^S \times V^S}{A_{280}^S \times V^S + A_{280}^P \times V^P}$ and $\frac{A_{280}^P \times V^P}{A_{280}^S \times V^S + A_{280}^P \times V^P}$) and are shown in Figure 2b. Compared with 1.5% SDS + 0.2% SC condition, the proportion of precipitate at 3.0% SDS + 0.2% SC condition significantly increased from 30.8% to 71.5%, indicating an increase in the separation efficiency of long SWCNTs. However, this increase in separation efficiency is mainly contributed by the precipitation of short SWCNTs, as shown in Figure 2c. Many short SWCNTs together with long SWCNTs precipitated, which indicates a decrease in the length resolution. Similar results were also observed for other controlled experiments, as shown in Figure 2d–f, in which the SC concentration was gradually increased from 0.2% to 2.0% at a fixed SDS concentration of 2%. Therefore, in the present binary-surfactant system, the separation efficiency of long SWCNTs is greater for high surfactant concentrations than for low surfactant concentrations, while the length resolution is lower. Furthermore, the present binary-surfactant system is also suitable for length separation of SWCNTs with different diameters synthesized by different methods (Figure S5, Supporting Information), indicating good universality. For the SWCNT materials with different diameter distributions, there is no significant difference in the surfactant concentration required for length separation. Despite this, we notice that the time required for precipitation of long SWCNTs is longer for small-diameter SWCNTs than for large-diameter SWCNTs (Figure S5, Supporting Information). This may be caused by their shorter lengths, compared with the large-diameter SWCNTs. For CoMoCAT SG65i SWCNTs with relatively narrow diameter- and chirality- distributions, the absorption baseline of the precipitate (long SWCNTs) was found to be much lower than that of the supernatant (short SWCNTs),

as shown in Figure S6 (Supporting Information). However, such a significant difference in absorption baseline between the supernatant and precipitate cannot be observed for arc-discharge SWCNTs due to their broad diameter- and chirality- distributions.

Generally, the surfactant coating on the nanotube surfaces is strongly dependent on the diameter and chirality of SWCNTs, which is an important foundation for diameter and chirality separation.^[22,48] However, no significant difference in optical absorption spectra was observed between the supernatant and precipitate at different surfactant concentrations (typical spectra are shown in Figure S7, Supporting Information), which indicated that there was no diameter- or chirality-selective precipitation of SWCNTs. Therefore, the present length-selective precipitation is not attributed to a change in the surfactants coated on the long-SWCNTs. This effect is possibly attributed to the state of the free surfactants in solution changing as the standing time increases, which mainly affects long SWCNTs. To gain insight into the mechanism of length-selective precipitation, we first performed a controlled experiment by using single-surfactant (SDS or SC) and binary-surfactant (SDS + SC) systems, in which the SDS or SC concentration was controlled to be the same between the two systems. Accordingly, we found that the long SWCNTs were precipitated only by the binary-surfactant system and not by the single-surfactant system (Figure 3a). Furthermore, at a specific concentration ratio between SDS and SC (such as 2:1), we found that the precipitation of SWCNTs did not occur at low surfactant concentrations (0.2% SDS + 0.1% SC and 0.4% SDS + 0.2% SC) but occurred at high surfactant concentrations (1.0% SDS + 0.5% SC, 2.0% SDS + 1.0% SC, and 4.0% SDS + 2.0% SC) (Figure 3b,c). In addition, the proportion of precipitate at an

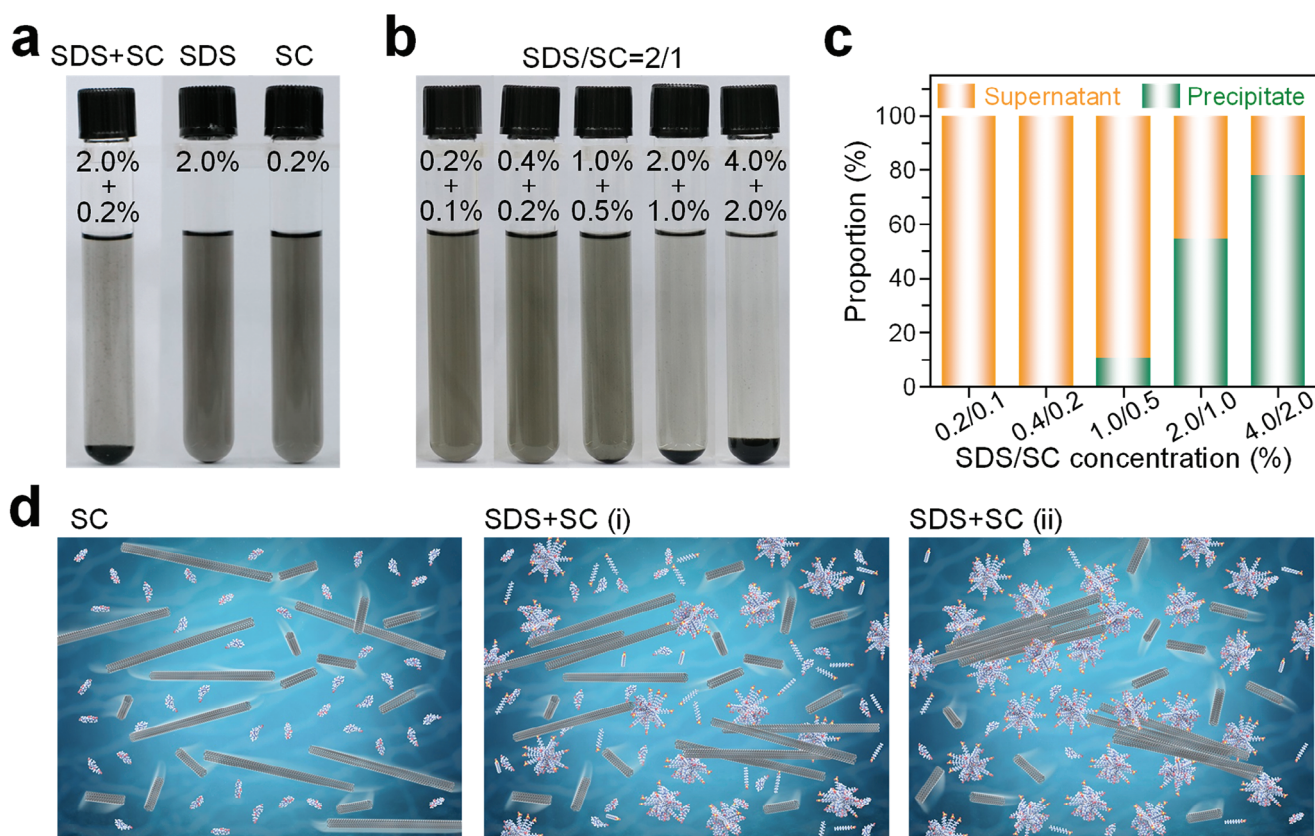


Figure 3. a) Photographs of SWCNT dispersions after 48 h of standing in a binary-surfactant system of 2% SDS + 0.2% SC (left), a single-surfactant system of 2% SDS (middle) and 0.2% SC (right). b) Photographs of SWCNT dispersions after 48 h of standing in a binary-surfactant system at different concentrations, in which the concentration ratio between SDS and SC was fixed at 2:1. c) Proportions of the supernatant and precipitate at different concentrations corresponding to b). d) Schematic diagrams for the proposed long and short SWCNTs dispersed in a single-surfactant system of SC (left) and a binary-surfactant system of SDS + SC (middle and right), in which “i” and “ii” indicate the early and late states, respectively.

appropriate 2.0% SDS + 1.0% SC condition was also found to increase with increasing SWCNT concentration (Figure S8, Supporting Information). These results reveal that the binary surfactant is an important factor for the selective precipitation of long SWCNTs. The spontaneous precipitation in the binary surfactant system may be influenced by other factors, such as the high concentration of SDS affecting the dissolution equilibrium of SC.

Generally, all single-surfactant molecules will be highly and uniformly dispersed in aqueous solution (unless the surfactant concentration is too high), and their presence does not obstruct or squeeze the suspended SWCNTs, as shown in Figure 3d. In contrast, the binary-surfactant molecules, especially SDS and SC surfactants, have been reported to easily form surfactant micelles due to strong interactions between the hydrophobic groups of SDS and SC, as demonstrated in previous theoretical experimental studies.^[22,46,49–51] The volume of each surfactant micelle is generally several times larger than that of a single surfactant. A larger volume may decrease the free volume available for individual SWCNTs, especially long SWCNTs. By referring to the model of molecular crowding reported by Zheng et al.,^[43] we propose that long SWCNTs with large excluded volumes are preferentially squeezed by the formed micelles rather than short SWCNTs and thus gradually form SWCNT clusters (the flocculent SWCNTs we observed), resulting in their final precipitation (Figure 3d). Sim-

ilar precipitation was also observed in the binary-surfactant systems of SDS and other cholate derivatives (such as sodium deoxycholate and sodium hydoxycholate) but not in the binary-surfactant systems of different cholate derivatives (Figure S9, Supporting Information). This result further verified our speculation of micelle-induced precipitation and suggested that chain-like SDS plays an important role in micelle formation. In contrast to the molecular crowding method reported previously,^[43] an additional crowding agent (polyethylene glycol) and additive (NaCl) are not needed in the present binary-surfactant system. This means that the long SWCNTs dispersed only in a binary-surfactant solution can be perfectly compatible with surfactant-based methods, including DGU, gel chromatography, and ATP, for various structure separations of SWCNTs. The present results are also very helpful for understanding the mechanism of structure separation of liquid-phase SWCNTs, in which not only the surfactants coated on nanotube surfaces but also the surfactants free in solution must be taken into account.

2.3. High-Efficiency and High-Resolution Length Separation

Based on the present binary-surfactant system, we designed a two-step precipitation process for high-resolution length

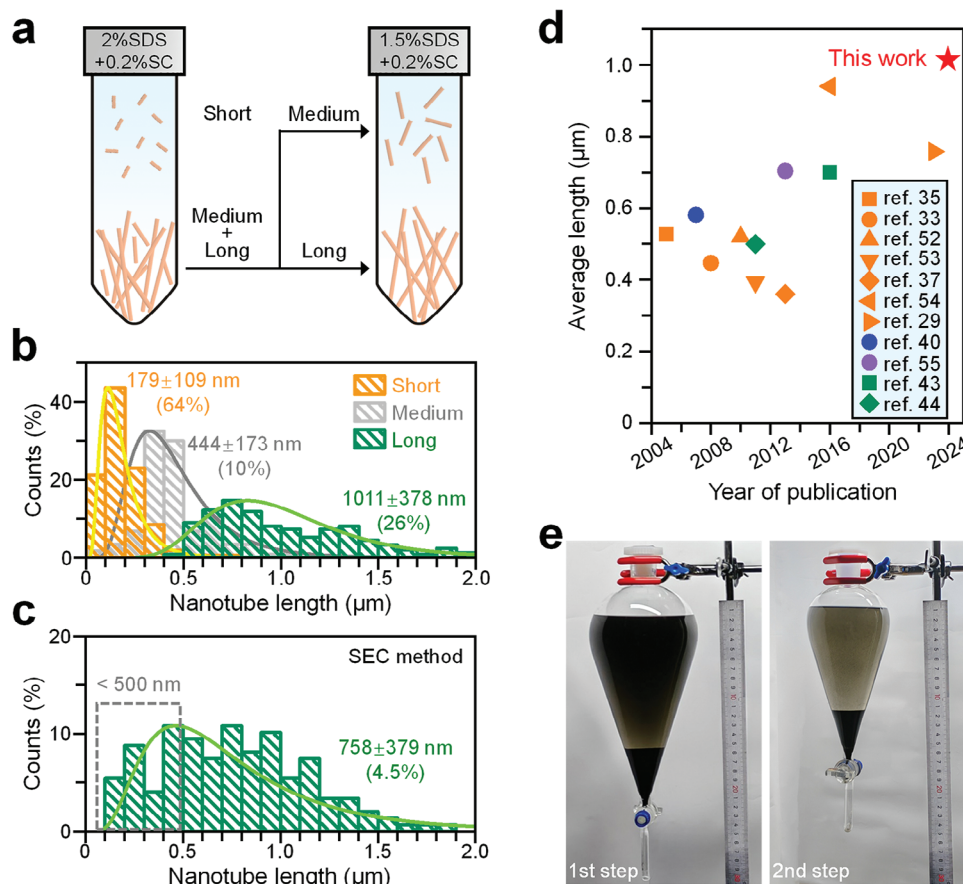


Figure 4. a) Schematic diagram of the two-step length separation process based on different surfactant concentrations. b) Length distributions of short, medium, and long SWCNTs obtained by the present method. c) Length distribution of long SWCNTs obtained by the traditional SEC method from ref.[29]. d) Comparison of the average length of long SWCNTs separated by different methods. e) Photographs of large-scale length-selective precipitation in the first step (1000 mL, left) and the second step (500 mL, right) corresponding to a).

separation of SWCNTs with narrow length distribution. As shown in **Figure 4a**, a relatively high surfactant concentration (2.0% SDS + 0.2% SC) was employed in the first step for precipitation of medium and long SWCNTs. After re-dispersing the precipitated SWCNTs, a relatively low surfactant concentration (1.5% SDS + 0.2% SC) was employed in the second step for precipitation of long SWCNTs. To fabricate high-performance TFTs, we further prepared semiconducting SWCNTs with an average diameter of 1.5 nm by using gel chromatography. The details of the separation will be reported elsewhere. From the optical absorption spectrum of the obtained semiconducting SWCNTs shown in **Figure S10** (Supporting Information), no obvious absorption peaks can be observed for metallic SWCNTs, indicating high semiconducting purity. Using the purified semiconducting SWCNTs, we performed length separation via two-step precipitation. **Figure 4b** shows the length distributions of the obtained short, medium, and long semiconducting SWCNTs; their average lengths were estimated to be 179 ± 109 , 444 ± 173 , and 1011 ± 378 nm, respectively. The typical AFM images are shown in **Figure S11** (Supporting Information). Compared with the long SWCNTs obtained by single-step precipitation using the conditions of 1.5% SDS + 0.2% SC and 2.0% SDS + 0.2%

SC (**Figure 2c,f**), the average length of the long SWCNTs obtained by two-step precipitation significantly increased. This difference is attributed mainly to the approximately perfect removal of short SWCNTs, which results in 99% of SWCNTs having lengths >500 nm. For comparison, the length distribution of long SWCNTs obtained by the traditional SEC method is also shown in **Figure 4c**,^[29] in which only 71% of SWCNTs are >500 nm in length. As shown in **Figure 4d**, the average lengths of SWCNTs separated by different methods were plotted for comparison.^[29,33,35,37,40,43,44,52–55] The data clearly show that the average length achieved by the present method significantly increased and reached a very high level. Although a higher average length (1.5 μm) was reported previously, this value may be overestimated due to the influences of nanotube bundles and alignment and thus was not considered here.^[56] On the other hand, for the short SWCNTs obtained by the present method, the percentage of SWCNTs <500 nm also reached 98%, further demonstrating that our present method has a clear advantage in length resolution compared with other methods reported previously.^[29,35,40,43] Furthermore, the separation efficiency of the present method (26% for long SWCNTs) is also much greater than that of the traditional SEC method (4.5%).^[29] Because the obtainable average length

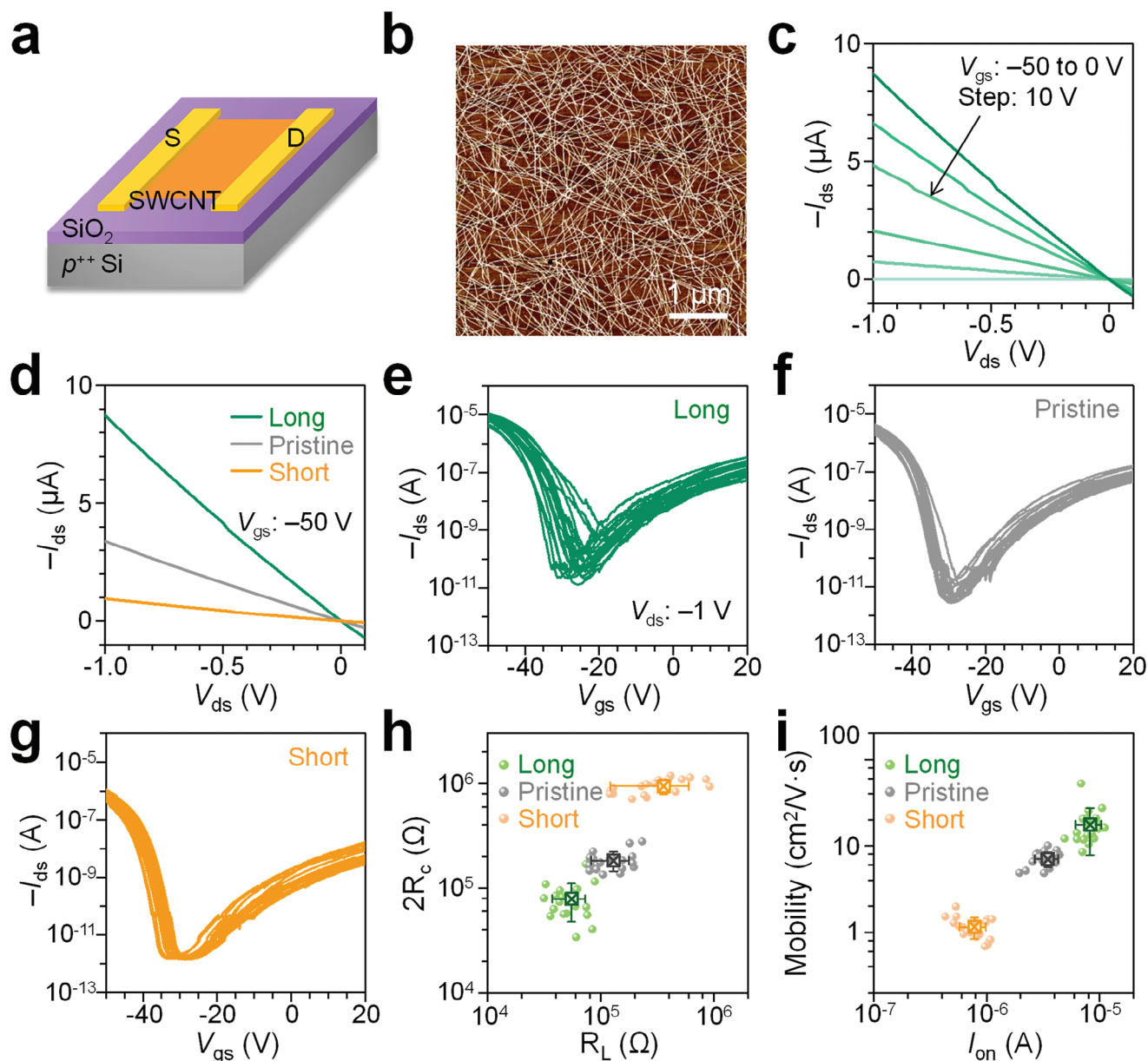


Figure 5. a) Schematic diagram of a back-gate TFT. b) A typical AFM image corresponding to the channel region. c) Typical output characteristic curves of TFTs fabricated with long semiconducting SWCNTs at different V_{gs} voltages measured under vacuum, in which the curve at V_{gs} of -10 V was magnified 10 times for easy distinction. d) Comparison of the output characteristic curves of TFTs fabricated with long, pristine, and short semiconducting SWCNTs at a V_{gs} of -50 V. (e–g) Transfer characteristic curves of TFTs fabricated with long e), pristine h), and short g) semiconducting SWCNTs, in which the V_{ds} voltage was fixed at -1 V. (h,i) Comparison of R_L and $2R_c$ (h), and I_{on} and mobility (i) of TFTs fabricated with long, pristine, and short semiconducting SWCNTs.

and separation efficiency based on length separation are also strongly dependent on the length distribution of the initially dispersed SWCNTs, it is possible to achieve the greater average length and separation efficiency by combining other high-efficiency and less-damaging dispersion methods for the preparation of long-SWCNT dispersions.^[57,58] In addition, unlike traditional methods with equipment requirements (such as SEC and DGU), the present method has very high scalability, which enables readily producing large-scale long SWCNTs, as shown in Figure 4e.

2.4. Improvement of Electrical Properties of Extracted Long Semiconducting SWCNTs

To investigate the difference in the electrical properties of separated long and short, and pristine (without length separation) semiconducting SWCNTs, we fabricated back-gate TFTs using these semiconducting SWCNTs, as shown in Figure 5a (the details on the manufacturing procedures are described in the Experimental Section). Figure 5b shows a typical AFM image corresponding to the channel region, in which long semiconducting

SWCNTs were randomly and uniformly deposited on the substrate. By modulating the deposition time of SWCNTs as we described previously,^[59] the linear densities of SWCNTs in channels composed of separated long and short, and pristine semiconducting SWCNTs were controlled to be ≈ 16 tubes μm^{-1} (Figure S12, Supporting Information) for a relatively reliable comparison of their electrical properties. As shown in Figure 5c and Figure S13 (Supporting Information), for any kind of semiconducting SWCNTs, the typical output characteristic curves measured under vacuum show a linear relationship between the source-drain current (I_{sd}) and voltage (V_{sd}), indicating ohmic contact between the SWCNTs and metal electrodes. Based on this, we estimated that the conductance ($I_{\text{sd}}/V_{\text{sd}}$) of long SWCNTs at a negative V_{gs} (-50 V) was 9.2 and 2.6 times greater than that of short and pristine semiconducting SWCNTs, respectively (Figure 5d). Figure 5e–g shows the transfer characteristic curves of TFTs fabricated with long, pristine, and short semiconducting SWCNTs. The uniformity of transfer characteristics is slightly worse for long SWCNTs than for pristine and short SWCNTs. Despite this effect, the difference in electrical properties is significant. For comparison, we further extracted the channel resistance (R_{L}), contact resistance between SWCNTs and two electrodes ($2R_{\text{c}}$), on-state current (I_{on}), and mobility from the transfer characteristic curves by using the Y function method described previously.^[60,61] As a result, the average value of R_{L} of long SWCNTs (55 k Ω) was estimated to decrease by 57.7% and 84.7% compared with that of pristine (130 k Ω) and short (360 k Ω) SWCNTs, respectively, while the average value of $2R_{\text{c}}$ (79 k Ω) was estimated to decrease by 57.0% and 91.6% compared with that of pristine (183 k Ω) and short (942 k Ω) SWCNTs, respectively (Figure 5h). The large difference in resistance is quite reasonable. Compared with short SWCNTs, the number of tube/tube junctions in the channel of long SWCNTs with similar linear densities significantly decreases, and the probability of SWCNTs directly bridging the source and drain electrodes increases, which results in improvements in the resistance of R_{L} and $2R_{\text{c}}$, respectively. Therefore, the average value of I_{on} for long SWCNTs (8.3×10^{-6} A) was estimated to increase by 2.4 and 10.5 times compared with that for pristine (3.5×10^{-6} A) and short (7.9×10^{-7} A) SWCNTs, respectively. In addition, the average value of mobility for long SWCNTs ($17.6 \text{ cm}^2 \text{ V}^{-1} \text{ s}^{-1}$) was also estimated to increase by 2.5 and 14.7 times compared with that for pristine ($7.1 \text{ cm}^2 \text{ V}^{-1} \text{ s}^{-1}$) and short ($1.2 \text{ cm}^2 \text{ V}^{-1} \text{ s}^{-1}$) SWCNTs, respectively (Figure 5i). It is clear that long SWCNTs exhibit better electrical properties than pristine and short SWCNTs. These electrical properties are comparable with previous reports based on other length separation methods.^[44,53,54] Furthermore, the electrical properties of SWCNT TFTs can be further improved by decreasing the channel length, increasing the linear density, and controlling the nanotube alignment.^[54] Although these experiments were beyond the scope of the present study, our results fully demonstrate the importance of the present technique for high-performance SWCNT-based devices.

3. Conclusion

In summary, we developed a straightforward, high-efficiency, and high-resolution method for the length separation of SWCNTs based on binary-surfactant systems. Our results clearly demon-

strate that long SWCNTs are selectively precipitated by modulating the concentration of binary surfactants. Through a systematic investigation of the effects of surfactant species and concentration, we revealed that the selective precipitation of long SWCNTs is induced by the effects of surfactant micelles, which significantly squeeze the free space of long SWCNTs due to the correspondingly larger excluded volumes than those of short SWCNTs. With the proposed two-step length separation method, we achieved the separation of near-pure long (≥ 500 nm in length, 99% in content) and short (≤ 500 nm in length, 98% in content) SWCNTs with separation efficiencies of 26% and 64%, respectively, indicating the advantages of the present method in terms of both length resolution and separation efficiency. Compared with TFTs fabricated from short semiconducting SWCNTs, TFTs fabricated from long semiconducting SWCNTs with an average length of ≈ 1 μm demonstrated significantly improved electrical properties, including a 10.5-fold on-state current and 14.7-fold mobility. Our present technique offers an effective strategy for the production of long SWCNTs with excellent properties and the subsequent fabrication of high-performance electronic and optoelectronic devices.

4. Experimental Section

Preparation of SWCNT Dispersion: Pristine arc-discharge SWCNTs (1.2–2.0 nm in diameter, Sigma-Aldrich) were used as the starting material without additional treatment. A 40 mg of SWCNT powder was dispersed in 40 mL of 1% SC (purity $\geq 99.0\%$, Sigma-Aldrich) aqueous solution by using a one-second on/off pulsed ultrasonic homogenizer (Sonifier 450D, Branson) at a power density of $\approx 30 \text{ W cm}^{-2}$ for 45 min (on-state time) at 15 $^{\circ}\text{C}$. After ultrasonication, the solution was ultracentrifuged for 1 h in an angle rotor (S50A, 50 000 rpm, Hitachi Koki) to remove catalytic metal particles, nanotube bundles, and impurities. The upper 80% of the supernatant was recovered as the SWCNTs dispersed in the single-surfactant system. Subsequently, the SDS (purity $\geq 99.0\%$, Sigma-Aldrich) surfactant was added to the SC-dispersed SWCNT solution to create a binary-surfactant system for length separation. To verify the effectiveness of the present length separation method, other SWCNT materials with different diameters, including plasma (0.9–1.7 nm in diameter, NanoIntegris), HiPco (0.7–1.0 nm in diameter, NanoIntegris), and CoMoCAT SG65i (0.78 nm in average diameter, Sigma-Aldrich) were also used for the preparation of SWCNT dispersions using the same ultrasonication and ultracentrifugation conditions.

Fabrication of Back-Gate TFTs: Length-separated long and short, and pristine semiconducting SWCNTs were used for the fabrication of back-gate TFTs using the same procedures described below. First, the SWCNTs were uniformly deposited on amine-functionalized SiO_2/Si substrates (300 nm thick for the SiO_2 layer) by using the NaHCO_3 control method reported previously.^[59] To remove the surfactants and NaHCO_3 coating on the nanotube surfaces, heat treatment was performed at 300 $^{\circ}\text{C}$ for 1 h and then at 500 $^{\circ}\text{C}$ for 1 h under vacuum. Source and drain electrodes (Ti/Pd: 0.5/40 nm) with a length of 10 μm and width of 20 μm were deposited via thermal evaporation (TE, SKY Technology) on the SWCNT film by standard photolithography (MA6, Zeiss). The SWCNTs outside the channel region were removed by oxygen plasma etching (RIE, Plasmalab 80 plus, Oxford Instruments).

Optical and Electrical Characterizations: Optical absorption spectra were measured from 1400 to 200 nm using an ultraviolet-visible near-infrared spectrophotometer (UV-3600, Shimadzu). Raman spectra were measured using a high-resolution confocal micro-Raman spectrometer (HRS-500SS, Princeton Instruments) equipped with a liquid nitrogen-cooled charge-coupled device detector (PYL-100BRX, Princeton Instruments). Two lasers of 633 and 532 nm were selected to excite the SWCNTs. The output and transfer characteristic curves of the fabricated TFTs were measured under vacuum using a Keithley 4200 system.

Supporting Information

Supporting Information is available from the Wiley Online Library or from the author.

Acknowledgements

S.L. and X.W. contributed equally to this work. This work was supported by the National Key Research and Development Program of China (grant nos. 2020YFA0714700 and 2018YFA0208402); National Natural Science Foundation of China (grant nos. 51820105002, 11634014, 51872320, and 52172060); Strategic Priority Research Program of Chinese Academy of Sciences (grant no. XDB33030100); Key Research Program of Frontier Sciences, CAS (grant no. QYZDBSSW-SYS028); and Youth Innovation Promotion Association of CAS (grant no. 2020005).

Conflict of Interest

The authors declare no competing financial interest.

Data Availability Statement

The data that support the findings of this study are available from the corresponding author upon reasonable request.

Keywords

length separation, selective precipitation, single-wall carbon nanotubes, size exclusion chromatography, surfactant micelle, thin-film transistors

Received: January 13, 2024

Revised: March 8, 2024

Published online:

- [1] Z. Xiao, W. Zhou, N. Zhang, Q. Zhang, X. Xia, X. Gu, Y. Wang, S. Xie, *Small* **2019**, *15*, 1804779.
- [2] X. Wei, S. Li, W. Wang, X. Zhang, W. Zhou, S. Xie, H. Liu, *Adv. Sci.* **2022**, *9*, 2200054.
- [3] X. Xia, Q. Zhang, W. Zhou, J. Mei, Z. Xiao, W. Xi, Y. Wang, S. Xie, W. Zhou, *Small* **2021**, *17*, 2102825.
- [4] J. Wu, L. Jiao, A. Antaris, C. L. Choi, L. Xie, Y. Wu, S. Diao, C. Chen, Y. Chen, H. Dai, *Small* **2013**, *9*, 4142.
- [5] S. Qiu, K. Wu, B. Gao, L. Li, H. Jin, Q. Li, *Adv. Mater.* **2019**, *31*, 1800750.
- [6] X. Zhang, J. Zhao, J. Dou, M. Tange, W. Xu, L. Mo, J. Xie, W. Xu, C. Ma, T. Okazaki, Z. Cui, *Small* **2016**, *12*, 5066.
- [7] M. Zhu, P. Lu, X. Wang, Q. Chen, H. Zhu, Y. Zhang, J. Zhou, H. Xu, Z. Han, J. Han, R. Chen, B. Li, L. M. Peng, Z. Zhang, *Small* **2023**, *19*, 2204537.
- [8] C. Qiu, Z. Zhang, M. Xiao, Y. Yang, D. Zhong, L. M. Peng, *Science* **2017**, *355*, 271.
- [9] T. Lei, Y. C. Lai, G. Hong, H. Wang, P. Hayoz, R. T. Weitz, C. Chen, H. Dai, Z. Bao, *Small* **2015**, *11*, 2946.
- [10] J. Gu, J. Han, D. Liu, X. Yu, L. Kang, S. Qiu, H. Jin, H. Li, Q. Li, J. Zhang, *Small* **2016**, *12*, 4993.
- [11] M. S. Arnold, S. I. Stupp, M. C. Hersam, *Nano Lett.* **2005**, *5*, 713.
- [12] M. S. Arnold, A. A. Green, J. F. Hulvat, S. I. Stupp, M. C. Hersam, *Nat. Nanotechnol.* **2006**, *1*, 60.
- [13] T. Tanaka, H. Jin, Y. Miyata, S. Fujii, H. Suga, Y. Naitoh, T. Minari, T. Miyadera, K. Tsukagoshi, H. Kataura, *Nano Lett.* **2009**, *9*, 1497.
- [14] H. Gui, H. Li, F. Tan, H. Jin, J. Zhang, Q. Li, *Carbon* **2012**, *50*, 332.
- [15] B. S. Flavel, M. M. Kappes, R. Krupke, F. Hennrich, *ACS Nano* **2013**, *7*, 3557.
- [16] C. Y. Khripin, J. A. Fagan, M. Zheng, *J. Am. Chem. Soc.* **2013**, *135*, 6822.
- [17] J. A. Fagan, E. H. Hároz, R. Ihly, H. Gui, J. L. Blackburn, J. R. Simpson, S. Lam, A. R. Hight Walker, S. K. Doorn, M. Zheng, *ACS Nano* **2015**, *9*, 5377.
- [18] H. Liu, D. Nishide, T. Tanaka, H. Kataura, *Nat. Commun.* **2011**, *2*, 309.
- [19] J. A. Fagan, C. Y. Khripin, C. A. Silvera Batista, J. R. Simpson, E. H. Haroz, A. R. Hight Walker, M. Zheng, *Adv. Mater.* **2014**, *26*, 2800.
- [20] G. Ao, C. Y. Khripin, M. Zheng, *J. Am. Chem. Soc.* **2014**, *136*, 10383.
- [21] H. Li, G. Gordeev, O. Garrity, S. Reich, B. S. Flavel, *ACS Nano* **2019**, *13*, 2567.
- [22] D. Yang, L. Li, X. Wei, Y. Wang, W. Zhou, H. Kataura, S. Xie, H. Liu, *Sci. Adv.* **2021**, *7*, eabe0084.
- [23] X. Luo, X. Wei, L. Liu, Z. Yao, F. Xiong, W. Zhou, S. Xie, H. Liu, *Carbon* **2023**, *207*, 129.
- [24] B. Podlesny, K. R. Hinkle, K. Hayashi, Y. Niidome, T. Shiraki, D. Janas, *Adv. Sci.* **2023**, *10*, 2207218.
- [25] S. Ghosh, S. M. Bachilo, R. B. Weisman, *Nat. Nanotechnol.* **2010**, *5*, 443.
- [26] X. Wei, T. Tanaka, Y. Yomogida, N. Sato, R. Saito, H. Kataura, *Nat. Commun.* **2016**, *7*, 12899.
- [27] G. Ao, J. K. Streit, J. A. Fagan, M. Zheng, *J. Am. Chem. Soc.* **2016**, *138*, 16677.
- [28] X. Wei, T. Tanaka, T. Hirakawa, M. Tsuzuki, G. Wang, Y. Yomogida, A. Hirano, H. Kataura, *Carbon* **2018**, *132*, 1.
- [29] X. Wei, X. Luo, S. Li, W. Zhou, S. Xie, H. Liu, *ACS Nano* **2023**, *17*, 8393.
- [30] H. Li, C. M. Sims, R. Kang, F. Biedermann, J. A. Fagan, B. S. Flavel, *Carbon* **2023**, *204*, 475.
- [31] H. Li, G. Gordeev, O. Garrity, N. A. Peyyety, P. B. Selvasundaram, S. Dehm, R. Krupke, S. Cambré, W. Wenseleers, S. Reich, M. Zheng, J. A. Fagan, B. S. Flavel, *ACS Nano* **2020**, *14*, 948.
- [32] L. Liang, W. Xie, S. Fang, F. He, B. Yin, C. Tlili, D. Wang, S. Qiu, Q. Li, *J. Mater. Chem. C* **2017**, *5*, 11339.
- [33] J. A. Fagan, J. R. Simpson, B. J. Bauer, S. H. De Paoli Lacerda, M. L. Becker, J. Chun, K. B. Migler, A. R. Hight Walker, E. K. Hobbie, *J. Am. Chem. Soc.* **2007**, *129*, 10607.
- [34] S. N. Barman, M. C. LeMieux, J. Baek, R. Rivera, Z. Bao, *ACS Appl. Mater. Interfaces* **2010**, *2*, 2672.
- [35] X. Huang, R. S. Mclean, M. Zheng, *Anal. Chem.* **2005**, *77*, 6225.
- [36] S. Park, H. W. Lee, H. Wang, S. Selvarasah, M. R. Dokmeci, Y. J. Park, S. N. Cha, J. M. Kim, Z. Bao, *ACS Nano* **2012**, *6*, 2487.
- [37] C. Y. Khripin, X. Tu, J. M. Heddlston, C. Silvera-Batista, A. R. Hight Walker, J. Fagan, M. Zheng, *Anal. Chem.* **2013**, *85*, 1382.
- [38] Y. Zhang, Y. Li, H. Wen, L. Cao, W. Xiao, J. Zhao, Z. Nan, S. Zhang, S. Qiu, Q. Li, *Carbon* **2023**, *215*, 118468.
- [39] H. Wen, J. Yao, Y. Li, Y. Li, L. Cao, W. Chi, Y. Wang, H. Jin, S. Qiu, J. Tang, Q. Li, *Nano Res.* **2023**, *16*, 1568.
- [40] J. A. Fagan, M. L. Becker, J. Chun, E. K. Hobbie, *Adv. Mater.* **2008**, *20*, 1609.
- [41] S. M. Tabakman, K. Welscher, G. Hong, H. Dai, *J. Phys. Chem. C* **2010**, *114*, 19569.
- [42] J. Chun, J. A. Fagan, E. K. Hobbie, B. J. Bauer, *Anal. Chem.* **2008**, *80*, 2514.
- [43] C. Y. Khripin, N. Arnold-Medabalimi, M. Zheng, *ACS Nano* **2011**, *5*, 8258.
- [44] H. Gui, H. Chen, C. Y. Khripin, B. Liu, J. A. Fagan, C. Zhou, M. Zheng, *Nanoscale* **2016**, *8*, 3467.
- [45] X. Wei, T. Tanaka, N. Akizuki, Y. Miyauchi, K. Matsuda, M. Ohfuchi, H. Kataura, *J. Phys. Chem. C* **2016**, *120*, 10705.
- [46] T. A. Shastry, A. J. Morris-Cohen, E. A. Weiss, M. C. Hersam, *J. Am. Chem. Soc.* **2013**, *135*, 6750.

- [47] X. Zeng, J. Hu, X. Zhang, N. Zhou, W. Zhou, H. Liu, S. Xie, *Nanoscale* **2015**, *7*, 16273.
- [48] L. Liu, X. Wei, Z. Yao, X. Li, W. Wang, Y. Wang, W. Zhou, F. Xiong, H. Kataura, S. Xie, H. Liu, *J. Phys. Chem. C* **2022**, *126*, 3787.
- [49] N. K. Subbaiyan, S. Cambré, A. N. Parra-Vasquez, E. H. Hároz, S. K. Doorn, J. G. Duque, *ACS Nano* **2014**, *8*, 1619.
- [50] S. Lin, D. Blankschtein, *J. Phys. Chem. B* **2010**, *114*, 15616.
- [51] B. Jójárt, M. Poša, B. Fiser, M. Szori, Z. Farkaš, B. Viskolcz, *PLoS One* **2014**, *9*, 102114.
- [52] Y. Miyauchi, K. Matsuda, Y. Yamamoto, N. Nakashima, Y. Kanemitsu, *J. Phys. Chem. C* **2010**, *114*, 12905.
- [53] Y. Asada, Y. Miyata, K. Shiozawa, Y. Ohno, R. Kitaura, T. Mizutani, H. Shinohara, *J. Phys. Chem. C* **2011**, *115*, 270.
- [54] F. Hennrich, W. Li, R. Fischer, S. Lebedkin, R. Krupke, M. M. Kappes, *ACS Nano* **2016**, *10*, 1888.
- [55] A. V. Naumov, D. A. Tsyboulski, S. M. Bachilo, R. B. Weisman, *Chem. Phys.* **2013**, *422*, 255.
- [56] Y. Miyata, K. Shiozawa, Y. Asada, Y. Ohno, R. Kitaura, T. Mizutani, H. Shinohara, *Nano Res.* **2011**, *4*, 963.
- [57] A. Graf, Y. Zakharko, S. P. Schießl, C. Backes, M. Pfohl, B. S. Flavel, J. Zaumseil, *Carbon* **2016**, *105*, 593.
- [58] P. Wang, M. Kim, Z. Peng, C. F. Sun, J. Mok, A. Lieberman, Y. Wang, *ACS Nano* **2017**, *11*, 9231.
- [59] W. Su, D. Yang, J. Cui, F. Wang, X. Wei, W. Zhou, H. Kataura, S. Xie, H. Liu, *Carbon* **2020**, *163*, 370.
- [60] Q. Cao, S. J. Han, G. S. Tulevski, A. D. Franklin, W. Haensch, *ACS Nano* **2012**, *6*, 6471.
- [61] W. Su, X. Li, L. Li, D. Yang, F. Wang, X. Wei, W. Zhou, H. Kataura, S. Xie, H. Liu, *Nat. Commun.* **2023**, *14*, 1672.